Yule-Nielsen based multi-angle reflectance prediction of metallic halftones

Vahid Babaei, Roger D. Hersch[*]

School of Computer and Communication Sciences
Ecole Polytechnique Fédérale de Lausanne (EPFL), Switzerland

ABSTRACT

Spectral prediction models are widely used for characterizing classical, almost transparent ink halftones printed on a diffuse substrate. Metallic-ink prints however reflect a significant portion of light in the specular direction. Due to their opaque nature, multi-color metallic halftones require juxtaposed halftoning methods where halftone dots of different colors are laid out side-by-side.

In this work, we study the application of the Yule-Nielsen spectral Neugebauer (YNSN) model on metallic halftones in order to predict their reflectances. The model is calibrated separately at each considered illumination and observation angle. For each measuring geometry, there is a different Yule-Nielsen n-value. For traditional prints on paper, the n-value expresses the amount of optical dot gain. In the case of the metallic prints, the optical dot gain is much smaller than in paper prints. With the fitted n-values, we try to better understand the interaction of light and metallic halftones.

Keywords: Multi-angle reflectance, metallic halftone, juxtaposed halftoning, BRDF, n-value, Yule-Nielsen modified spectral Neugebauer model (YNSN)

1. INTRODUCTION

Printer characterization enables establishing a color reproduction workflow[1]. Printer characterization creates a relationship between area coverages of the inks and the color of the printed halftones. The mapping between area coverages of inks and resulting color allows computing the gamut volume, performing the color separation and, ultimately, printing a desired image. This mapping can be established with spectral prediction models.

Spectral prediction models are widely used for characterizing classical, almost transparent ink halftones printed on a diffuse substrate. However, there are applications where the inks or the substrate are not diffuse. For example, metallic-ink prints reflect most of the light in the specular direction. Due to their opaque nature, multi-color metallic halftones require juxtaposed halftoning methods[2-4], where halftone dots of different colors are laid out side-by-side.

We are interested in predicting the reflectances and colors of metallic halftone prints for different illumination and observation geometries. Multi-angle spectral measurement devices enable measuring the reflectances at a number of different illumination and observation geometries.

[*]Authors e-mail addresses: vahid.babaei@epfl.ch and rd.hersch@epfl.ch

In the present paper, we study the Yule-Nielsen modified spectral Neugebauer model (YNSN) for predicting the reflectances of metallic halftones calibrated separately for each of the different illumination and observation orientations. We observe the model prediction accuracy as well as the best Yule-Nielsen n-value for the different measuring geometries. For traditional prints on paper, the n-value expresses the amount of optical dot gain. By analyzing the Yule-Nielsen graphs, we try to better understand the interaction of light and halftones of multi-chromatic metallic prints.

2. PREVIOUS WORK

To the best of our knowledge, no prior work addresses the color prediction of halftone prints composed of multi-chromatic metallic inks. Existing technologies comprise prints where transparent inks are deposited on a silver ink[5] or on a metallic sheet[6]. For such prints there have been attempts to establish color prediction models for viewing the prints at non-specular observation angles[7, 8]. In respect to the prediction of color in specular viewing mode, Pjanic and Hersch[6] used a cellular YNSN model in order to characterize metallic color prints made of transparent inks deposited on a metallic sheet. In order to reproduce the BRDF of flat surfaces, Matusik *et al.*[9] combined by halftoning the BRDFs of metallic and non-metallic inks.

3. EXPERIMENTAL SETUP

To perform spectrophotometric measurements for different illumination and viewing geometries, we used the MA98, a multi-angle spectrophotometer from X-Rite. It has two illuminants at 15° and 45° with respect to the surface normal and sensors inside and outside of the plane of incidence located at the angles proposed by Alman[10]. In the present experiments, we consider only the 45° incident illumination. The available measurement geometries of the MA98 device are summarized in Table III of the Appendix.

Nowadays, printing technologies such as offset and gravure are capable of printing with metallic inks. However, experimenting with these technologies is prohibitively expensive. We use the OKI DP-7000 printer (also known as ALPS MD) to print metallic inks. The printer can print with up to 9 inks at once. The inks include process, metallic and spot colors. The printer uses a thermal transfer technology. The inks are transferred to the substrate by heating a ribbon. In this work, we use only the 4 available metallic inks: metallic cyan (*c*), metallic magenta (*m*), gold (*y*) and silver (*s*). In order to generate metallic halftones, we apply discrete line juxtaposed halftoning[4].

The OKI DP-7000 can nominally print up to a resolution of 1200 dpi. However, our registration tests indicated that for high frequency patterns, even the minimum printer resolution of 300 dpi does not prevent considerable overlaps between juxtaposed ink layers. Therefore, in all our experiments we consider an effective resolution of 100 dpi by forming pixels made of 3×3 squares at 300 dpi nominal resolution.

4. SPECTRAL COLOR PREDICTION OF METALLIC HALFTONES

In order to establish a color reproduction workflow, a spectral prediction model enables calculating the color gamut and establishing the color separation tables without requiring many measurements. A prediction model is especially interesting for metallic halftones since it allows characterizing metallic prints at different illumination and observing angles by measuring only a limited number of calibration samples. In this section, we study the application of the well-known Yule-Nielsen modified spectral Neugebauer (YNSN) prediction model for predicting the color of metallic halftones. This model is easy to calibrate and doesn't require that the inks are transparent.

4.1 Yule-Nielsen spectral Neugebauer prediction model

The Yule-Nielsen modified spectral Neugebauer model[11] predicts the overall reflectance $R(\lambda)$ of a halftone as a weighted average of the colorant reflectances $R_i(\lambda)$ in a power function space:

$$R(\lambda) = \left(\sum_i a_i R_i(\lambda)^{1/n} \right)^n \qquad (1)$$

where a_i is the fractional area coverage of fulltone colorant i. In the general case, fulltone colorants are the unprinted paper, the fulltone inks and all possible superpositions of fulltone inks. Fulltone colorants are also called Neugebauer primaries. For opaque metallic inks, we consider as colorants only the fulltone inks. For classical prints on paper, the n-value accounts for the optical dot gain due to lateral propagation of light inside the substrate and to multiple internal reflections between the paper bulk and the print-air interface. The n-value is optimized by considering a limited number of measured sample reflection spectra.

When using the YNSN model for predicting the reflectance of discrete line juxtaposed halftones[4], the spreading of the ink dots is unknown[12]. Since the resolution is low, we use as effective area coverage the nominal area coverages of the contributing halftone colorants.

4.2 Prediction accuracy of the YNSN model for juxtaposed metallic-ink halftones

In order to examine the prediction accuracy of the YNSN model for metallic-ink halftones, we consider a test set formed by variations of the nominal surface coverages of the four metallic inks in 20% intervals while constraining them such that the sum of the area coverages remains one, i.e. $c + m + y + s = 100\%$, where c, m, y and s denote the respective area coverages of the cyan, magenta, yellow and silver inks. This yields 56 combinations of four area coverages that are rendered using discrete line juxtaposed halftoning. Figure 1 shows an example of a discrete line juxtaposed halftone screen incorporating discrete line colorants placed side by side. It also shows the repetitive halftone screen element formed by a parallelogram composed of discrete line segments. Note that for our spectral measurements, the plane of incidence is horizontal, i.e. parallel to the x-axis.
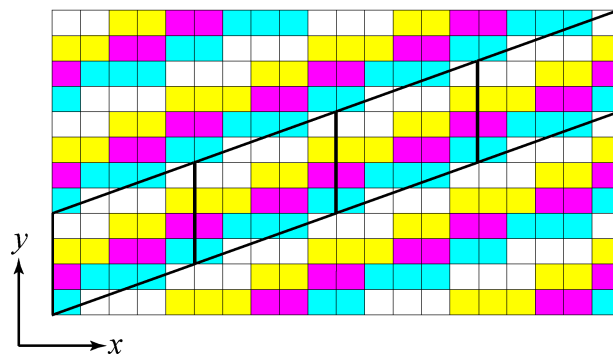

Figure 1. A juxtaposed halftone line screen comprising four colorants with different area coverages: c 25%, m 20%, y 25% and s 30%. The corresponding parallelogram screen elements boundaries are shown with a solid line.

Table I summarizes the prediction accuracies for all 11 geometries. Note that the best n-value for each geometry is obtained by minimizing the average RMS difference between the 56 spectral reflectance measurements and their

predicted counterparts. We allowed the *n*-value to vary between -10 to 10 at 0.1 intervals. Values greater than 10 or less than -10 do not change the results significantly and can be considered as infinity[13].

As shown in Table I, the prediction accuracy of the YNSN model, expressed as CIEDE2000 color difference[16], is within an acceptable range. The color accuracy varies according to the measuring geometry. This is partially due to the magnitudes of the reflectance factors of the metallic inks that vary greatly according to the different measuring geometries. When using the diffusing white spectralon at 45 as 45 (45° aspecular 45° corresponding to, 45°:0°) as white reference for computing the CIELAB color coordinates, for near specular geometries, we reach higher CIELAB values. On the other hand, for small reflectance values (compared to the reference white) of far from specular geometries, we obtain systematically low CIELAB values. Hence, the color differences are biased and depend on the relative amplitude of the reflectances.

Table I. The prediction accuracy of the YNSN model calibrated separately for each measuring geometry under the D65 illuminant for a test set of 56 discrete line juxtaposed halftones. The white reference is either the diffuse white of a spectralon sample measured at 45 as 45 (45°:0°) or the solid silver ink measured at each corresponding geometry.

Test set	Geometry	Mean ΔE_{00} (spectralon)	Mean ΔE_{00} (silver)	Mean NED %	*n*-value
56 discrete line juxtaposed metallic-ink halftones	45 as -15 (45°:60°)	3.07	2.33	4.73	-2.2
	45 as 0 (45°:45°)	2.34	1.67	4.19	8.2
	45 as 15 (45°:30°)	0.82	0.74	2.29	1.4
	45 as 25 (45°:20°)	1.16	1.14	3.19	1.0
	45 as 45 (45°:0°)	2.68	3.32	6.18	0.6
	45 as 75 (45°:-30°)	2.23	3.20	7.14	0.6
	45 as 110 (45°:-65°)	2.05	3.13	7.13	0.6
	45 as 25 az 90	1.42	1.39	3.99	1.4
	45 as 25 az -90	1.35	1.34	3.60	1.6
	45 as 60 az 125.3	1.56	2.03	4.32	0.7
	45 as 60 az -125.3	1.60	2.11	4.52	0.7

As an alternative to the diffuse white substrate, we also use as white reference the silver reflectance measured at each corresponding geometry. Although this is reasonable for near specular geometries, for far from specular geometries the silver reflectance is low and is not anymore the brightest point on which the eye adapts. To account for this, in Table I, we propose a metric based on the Euclidean distance between two spectral reflectance vectors normalized in respect to the measured spectral reflectance. We call it *normalized Euclidean difference* (NED) and define it as

$$\text{NED} = \frac{\left| R_m - R_p \right|}{\left| R_m \right|} \qquad (2)$$

where R_m is the measured spectral reflectance represented as a 36-vector (from 380 to 760 nm with 10nm intervals), R_p the predicted reflectance spectrum (also a 36-vector) and operator $|\,|$ gives the Euclidian length. This metric shows the proximity of a predicted spectrum to the measured one independently of the spectrum magnitude.

According to the NED metric in Table I, for geometries near to specular, the prediction accuracy is higher than for geometries far from it. We observe low prediction accuracies for the 45 as 75 (45°:-30°) and the 45 as 110 (45°:-

65°) geometries. The best prediction accuracy is obtained for capturing angles between the specular (45°:45°) and the normal (45°:0°) orientation such as 45 as 15 (45°:30°) and 45 as 25 (45°:20°).

4.3 Yule-Nielsen *n*-value for different geometries

Let us analyze how the optimal *n*-values behave as a function of the measuring geometry. We examine one halftone sample with 60% metallic magenta and 40% silver. The prediction accuracies for this particular halftone are collected in Table II. As shown in this table, there are different optimal *n*-values for different geometries. For the 45 as -15 geometry, extending our study to negative *n*-values proved to be helpful. In addition, 5 out of the 11 geometries have an optimized *n*-value in the interval (0, 1) which is rather unusual.

Table II. The prediction accuracy of the YNSN model for a single discrete line juxtaposed halftone (*m* 0.6, *s* 0.4) calibrated separately for each measuring geometry.

Test set	Geometry	ΔE_{00} (spectralon)	ΔE_{00} (silver)	NED %	*n*-value
A halftone composed of 60% metallic magenta and 40% silver	45 as -15 (45°:60°)	2.67	2.22	5.38	-2.1
	45 as 0 (45°:45°)	0.32	0.28	0.71	2.5
	45 as 15 (45°:30°)	0.87	0.78	1.92	2.1
	45 as 25 (45°:20°)	0.44	0.44	0.79	1.2
	45 as 45 (45°:0°)	0.85	0.90	2.95	0.8
	45 as 75 (45°:-30°)	1.81	2.19	4.87	0.6
	45 as 110 (45°:-65°)	1.91	2.34	5.34	0.6
	45 as 25 az 90	0.53	0.51	1.52	1.1
	45 as 25 az -90	0.59	0.59	1.44	1.5
	45 as 60 az 125.3	1.70	1.95	4.21	0.7
	45 as 60 az -125.3	0.69	0.83	2.12	0.8

4.4 Analysis of the Yule-Nielsen function

In order to better understand the effect of different *n*-values on the prediction of halftone reflectances, we use the graphical representation of the Yule-Nielsen (YN) function[14]. For a two-colorants metallic halftone, we denote $R_a(\lambda)$ the spectral reflectance of the halftone patch composed of the metallic non-silver ink with coverage *a* ($0<a<1$) and the silver ink with area coverage ($1-a$). $R_1(\lambda)$ is the spectral reflectance of the non-silver metallic ink with full area coverage. The silver ink is assimilated to the "white" background with reflectance $R_0(\lambda)$. The YN function for this halftone is

$$R_a\left(\lambda\right)=\left[\left(1-a\right)R_0^{1/n}\left(\lambda\right)+aR_1^{1/n}\left(\lambda\right)\right]^n. \qquad (3)$$

By dividing Eq. (3) by $R_0(\lambda)$ we obtain for each wavelength

$$R_a/R_0=\left[1-a+a\left(R_1/R_0\right)^{1/n}\right]^n. \qquad (4)$$

The relative attenuation of the halftone R_a/R_0 as a function of the relative attenuation of the fulltone R_1/R_0 can be plotted according to the spectral measurements of $R_0(\lambda)$, $R_a(\lambda)$ and $R_1(\lambda)$. These reflectances provide as many R_a/R_0 and R_1/R_0 attenuations as discrete values contained in the measured spectra.

In Figure 2 we show the YN function for a halftone area coverage of $a = 0.6$ and for different values of n. The straight line with $n = 1$ represents the "Neugebauer function", a linear relationship between no attenuation and attenuation by the fulltone ink according to the area coverage of that ink. Varying the n-value has the effect of making the YN function nonlinear. The traditional interval of n-values [1, 100] covers a small portion of the function's range. In this interval, the reflectance of halftones is lower than the one predicted by the Neugebauer function. Extending this interval to negative values[13] helps spanning a greater portion of the range. The most interesting case is the interval (0, 1) where the YN function yields an inverse effect, i.e. the halftone exhibits a higher reflectance than the one predicted by the Neugebauer function.
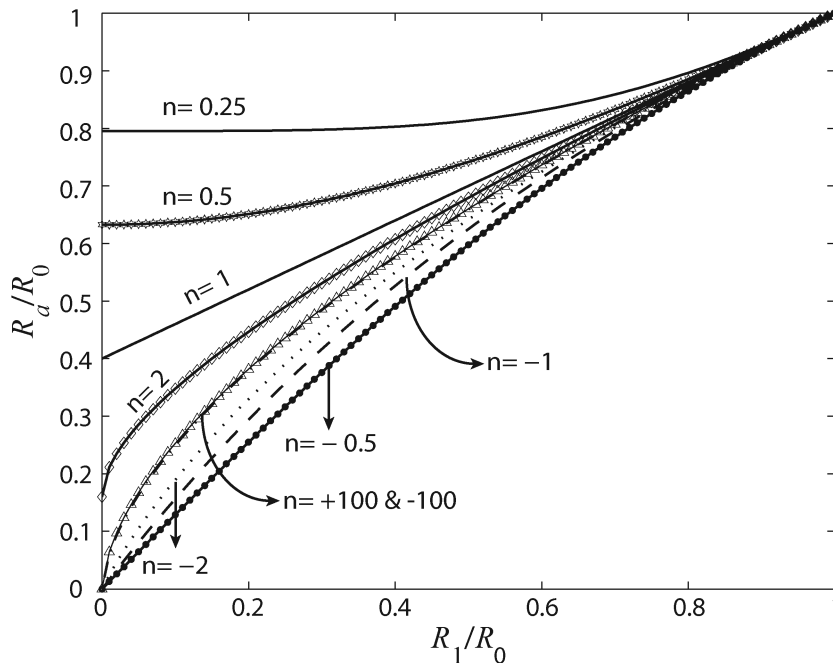

Figure 2. The Yule-Nielsen graph for different n-values for the non-silver halftone area coverage of $a = 0.6$. Note that the $n = 100$ and $n = -100$ curves nearly coincide.

Let us study the metallic halftone ($m = 0.6$, $s = 0.4$) using the fitted YN function along with measured data for some representative geometries. Figure 3 shows the function for three n-values: $n = 1$ which represents the Neugebauer function, $n = 2$ as recommended by Yule and Nielsen[15], and the best fitted n-value according to Table II. Depending on the measuring geometry, the value R_1/R_0 can be larger than 1. Also, some R_a/R_0 values can be above the Neugebauer line, yielding fitted n-values between 0 and 1.

We observe that for all geometries the measured attenuations follow a straight line. This is in contrast with a traditional print on paper where due to optical dot gain the halftone attenuation follows a curve similar to the $n = 2$ Yule-Nielsen curve. This might be an indication of a very moderate or no optical dot gain.

4.5 Yule-Nielsen *n*-value as a compensating factor for shadowing and misregistration

In traditional prints with transparent inks on a diffusely reflecting paper, the n-value accounts for the nonlinear effects occurring due to sub-surface scattering and multiple reflections between the paper bulk and the print-air

interface. For such prints, the halftone attenuation forms a curve similar to the YN function, generally with $1 < n < 100$.

In our experiments the metallic flakes reflect strongly at specular angles and weakly at non-specular angles. They are printed at a very low print resolution and cover the full surface. Therefore, optical dot gain induced by scattering of light in the paper substrate is not likely to occur. A simple Neugebauer model could be enough for predicting these halftone reflectances. But why do we have n-values different from 1? And, why are the n-values different for different measuring geometries?
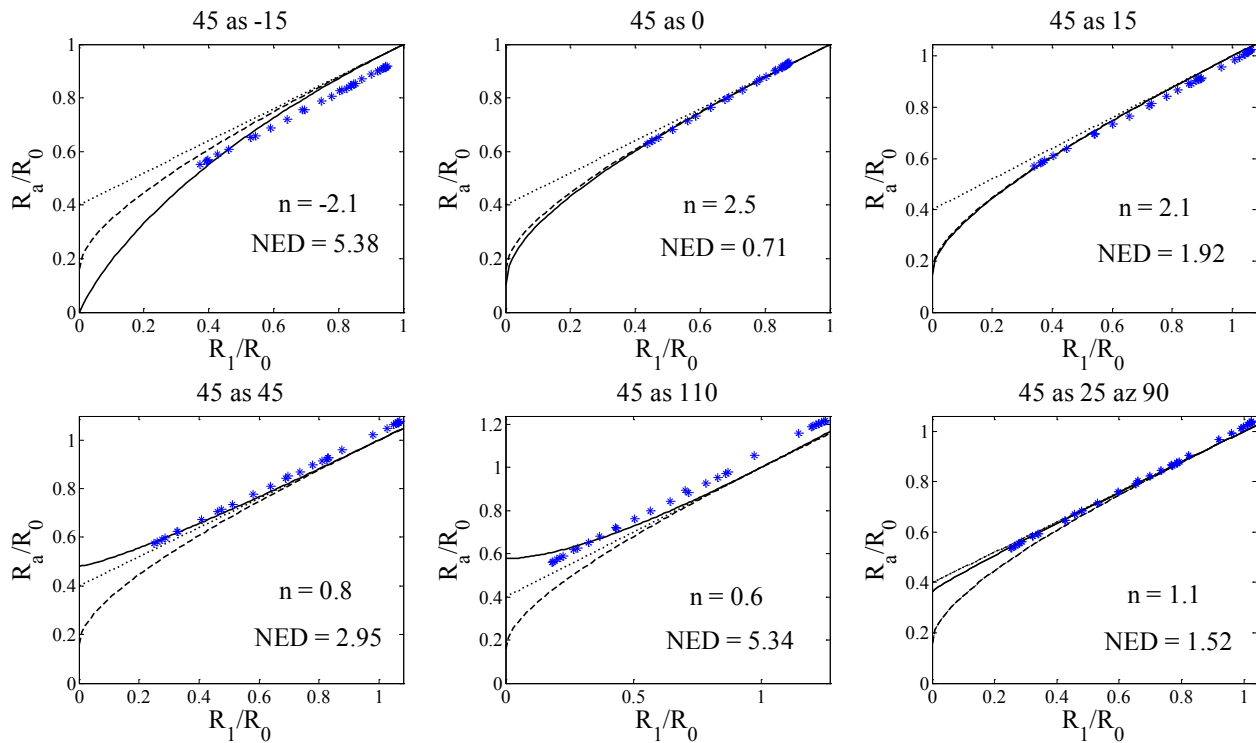

Figure 3. Measured halftone attenuation and Yule-Nielsen graphs for different geometries. The YN function graphs are plotted for $n = 1$(dotted line), $n = 2$ (dashed line) and the fitted n (solid line) of the halftone ($m = 0.6$, $s = 0.4$). The fitted n-value for each graph is written inside the plots.

To investigate these questions, we designed an experiment that demonstrates the effect of juxtaposed halftoning on the texture of a metallic sample and on its multi-angle reflection behavior. Figure 4 shows the microscopic image of two samples. In Figure 4a we have a fulltone (100%) metallic magenta sample printed in a single pass. To simulate the effect of halftoning, in Figure 4b, we try to generate the same fulltone magenta sample but by sequentially printing four halftone lines of metallic magenta side by side. Without the effects of multi-pass printing, the two samples would have the same reflection spectra at all illumination and observation angles. However, from the microscopic images we can observe the differences. In the "multi-pass" fulltone magenta sample, the misregistration between successive printed lines generates small unprinted white areas. In addition, the partial superposition of the halftone lines due to misregistration makes the surface of the multi-pass solid magenta uneven and prone to shadowing.

Figure 5 shows the reflectance spectra of the two samples depicted in Figure 4. The difference between the two reflectance spectra depends on the measuring geometry. Note that in the case of the traditional 45 as 45 (45°:0°)

geometry, there is an identical spectrum for both samples. This indicates that, at this non-specular geometry, the multi-pass "texture" has no effect. On the other hand, for measurement geometries close to specular, the texturing effect of the multi-pass printing is high.
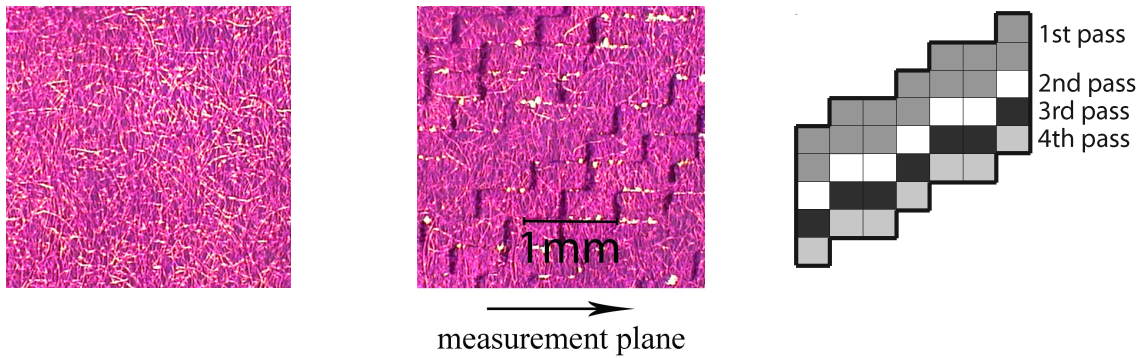

Figure 4. The microscopic image of 100% metallic magenta taken in transmission mode: (a) printed in one pass; (b) printed in 4 passes by printing several discrete lines side by side and (c) the layout of one halftone screen element used for generating the multi-pass solid magenta sample.
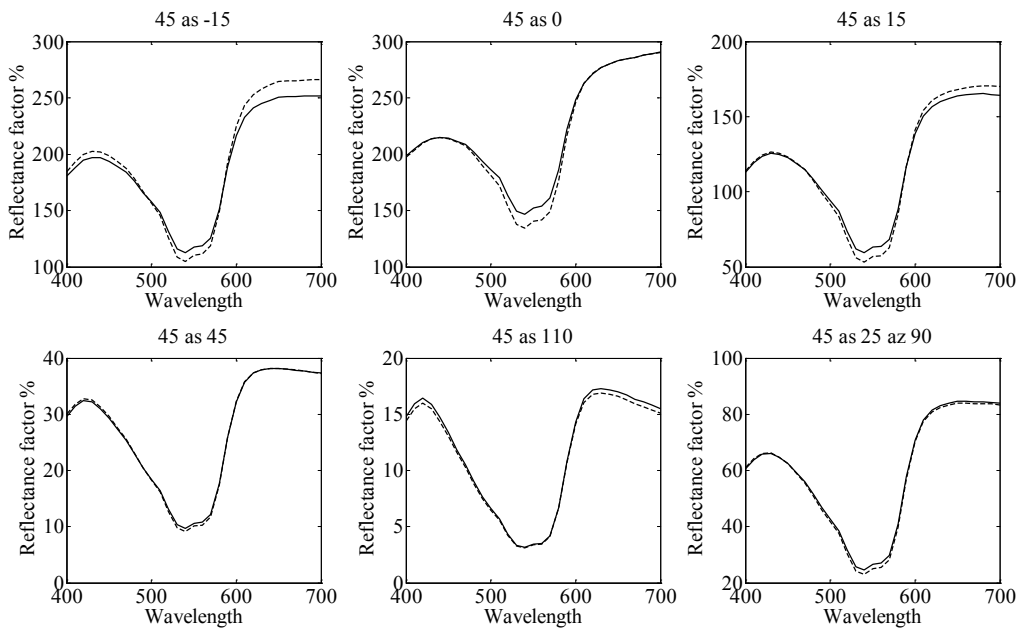

Figure 5. The spectral reflectances for solid 100% magenta (solid line) and for the multi-pass 100% magenta (dashed line) for some representative geometries. The measurements have taken place with our default setup, i.e. the plane of incidence of the MA98 spectrophotometer is parallel to the horizontal axis of the halftones.

Slight shifts between the colorant layers may explain the need for Yule-Nielsen n-values which vary in function of the measurement geometry. Note that misregistration also occurs in classical prints. However, since classical inks are transparent and since their halftone dots partially overlap, the misregistration effect is weak. Depending on the measuring geometry, the metallic halftones exhibit different contributions of shadowing and white interstices.

Misregistration creates shadowing effects which result in darker measurements and unprinted space between halftone dots that lighten the reflectance. The *n*-value seems to account for these two inverse effects. Since the effects of shadowing and white interstices are different for each geometry, the *n*-value also differs.

5. CONCLUSIONS

In order to create a color reproduction workflow for metallic inks, one needs to characterize the metallic halftones, possibly accounting for several illumination and observation geometries. Such a characterization enables simulating the appearance of the final print at different observation conditions.

The printer characterization is performed with a spectral prediction model. We investigated the Yule-Nielsen spectral Neugebauer spectral prediction model for the different measurement geometries. This prediction model, calibrated separately for each geometry, shows a good color prediction accuracy. The Yule-Nielsen *n*-value varies for each geometry and accounts for effects induced by colorant misregistration such as shadows and white interstices at halftone dot borders.

REFERENCES

[1] Morovič J. and Lammens J., "Color management," in [Colorimetry: Understanding the CIE System], Ed. Schanda J., J. Wiley, Chapter 7, 159–206 (2007).

[2] Morovič J., Morovič P. and Arnabat J., "HANS: Controlling ink-jet print attributes via Neugebauer primary area coverages," IEEE Trans. Image Process., 21 (2), 688–696 (2012).

[3] Ostromoukhov V. and Hersch R. D., "Multi-color and artistic dithering," Proc. SIGGRAPH 99, in Computer Graphics Proceedings, Annual Conference Series, 425–432 (1999).

[4] Babaei V. and Hersch R. D., "Juxtaposed color halftoning relying on discrete lines," IEEE Trans. Image Process., 22 (2), 679–686 (2013).

[5] Ainge A., "Improvements in printing processes using metallic inks," European Patent Application EP1517797 (2003).

[6] Pjanic P. and Hersch R. D., "Specular color imaging on a metallic substrate," Proc. IS&T 21st Color Imaging Conference, 61–68 (2013).

[7] Hersch R. D., Collaud F. and Emmel P., "Reproducing color images with embedded metallic patterns," Proc. SIGGRAPH, ACM Trans. on Graphics, 22 (3), 427–436 (2003).

[8] Bugnon T., Maesani A. and Hersch R. D., "Enhancing the specular effect of metallic color prints by reducing the use of yellow ink," J. Imaging Sci. Techn., 55 (6), 060506-1–060506-9 (2011).

[9] Matusik W., Ajdin B., Gu J., Lawrence J., Lensch H. P. A., Pellacini F. and Rusinkiewicz S., "Printing spatially-varying reflectance," ACM Trans. on Graphics, 28 (3), 128:1–128:9 (2009).

[10] Alman D. H., "Directional color measurement of metallic flake finishes," Proc. Inter-Society Color Council Conference on Appearance, Williamsburg, 53–56 (1987).

[11] Viggiano J. A. S., "Modeling the color of multi-colored halftones," Proc. TAGA, 42, 44–62 (1990).

[12] Babaei V. and Hersch R. D., "Spectral prediction of juxtaposed halftones relying on the two-by-two dot centering model," J. Imaging Sci. Techn., 57 (4), 040501-1–9 (2013).

[13] Lewandowski A., Ludl M., Byrne G. and Dorffner G., "Applying the Yule-Nielsen equation with negative n," J. Opt. Soc. Amer. A, 23 (8), 1827–1834 (2006).

[14] Hébert M., "Yule-Nielsen effect in halftone prints: graphical analysis method and improvement of the Yule-Nielsen transform," Proc. SPIE 9015, Color Imaging XIX: Displaying, Processing, Hardcopy, and Applications (2014).

[15] Yule J. A. C. and Nielsen W. J., "The penetration of light into paper and its effect on halftone reproduction," Proc. TAGA, 3, 65–76 (1951).

[16] Luo M. R., Cui G. and Rigg B., "The development of the CIE 2000 colour-difference formula: CIEDE2000," Color Res. Appl., 26 (5), 340–350 (2001).

APPENDIX

Table III. Measuring geometries provided by the X-Rite MA98 spectrophotometer.

Illumination	Viewing (aspecular, azimuth)	Illumination	Viewing (aspecular, azimuth)
45	-15, 0	15	-45, 0
45	0, 0	15	-15, 0
45	15, 0	15	15, 0
45	25, 0	15	45, 0
45	45, 0	15	80, 0
45	75, 0	15	38.3, 43
45	110, 0	15	38.3, -43
45	25, 90	15	46.9, 104.5
45	25, -90	15	46.9, -104.5
45	60, 125.3	--	--
45	60, -125.3	--	--